NASA Technical Paper 2755

September 1987

Permeation of Oxygen Through High Purity, Large Grain Silver

R. A. Outlaw,
W. K. Peregoy,
and Gar B. Hoflund

NASA

NASA Technical Paper 2755

1987

Permeation of Oxygen Through High Purity, Large Grain Silver

R. A. Outlaw
and W. K. Peregoy
Langley Research Center
Hampton, Virginia

Gar B. Hoflund
University of Florida
Gainesville, Florida

National Aeronautics
and Space Administration

Scientific and Technical Information Office

Introduction

The concept of generating a laboratory atomic oxygen beam for testing materials and coatings that are to experience long-term space exposure has been previously reported (ref. 1). This concept primarily involves two sequential mechanisms: (a) permeation of oxygen atoms through silver, which ultimately adsorb at the ultrahigh vacuum (UHV) interface, and (b) electron stimulated desorption, which is a flux of low-energy electrons (~100 eV) impinging on the interface, exciting the atoms to antibonding states, and ultimately resulting in desorption of hyperthermal neutral atoms (~5 eV). In order to achieve a sufficient flux of atomic oxygen to simulate what is experienced in orbit ($\sim 10^{-15}$ cm^{-2}-s^{-1}), it is necessary to maximize the oxygen transport through Ag. Since there is virtually no information as to whether the transport is primarily by grain boundary diffusion or volume diffusion, it is important to study this system so that the Ag membrane microstructure can be appropriately tailored to provide maximum flux.

Past experiments directed toward the measurement of the diffusivity of oxygen in Ag have employed either the desorption technique, the electrochemical technique, or the permeation technique, but interestingly, in all cases, the effects of grain boundary density and material purity have not been addressed (refs. 2 through 7). If grain boundary diffusion is a significant part of the transport mechanism for the diffusion of oxygen in Ag, then grain boundary density would have a major effect. Experiments with larger grain size would reduce the number of transport paths and would provide smaller permeation rates compared with past research (which most likely had small grains and therefore higher grain boundary densities). Further, the segregation of impurities (both species and amount) to grain boundaries could cause diffusivity variations.

An important feature of the permeation technique used in this work is that bulk cleanup of the material studied is much more probable because of the very thin membranes used (~0.254 mm). Segregation of the impurities to grain boundaries and then to the free surface can occur much faster, thus a more rapid cleanup by oxidation and desorption of reaction products is provided. The purpose of this paper is to report data for the permeation of oxygen through high purity, large grain silver membranes; UHV conditions are used to serve as a basis for comparison with past research and to provide some insight into the aforementioned effects.

Symbols and Abbreviations

A	membrane area, cm^2
AES	Auger electron spectroscopy
C	concentration, number of oxygen atoms per cm^3 of Ag, cm^{-3}
D	diffusivity, cm^2-s^{-1}
d	membrane thickness, cm
E	energy, erg (6.95×10^{-13} times energy in kcal-mole^{-1})
E_a	activation energy, erg (6.95×10^{-13} times energy in kcal-mole^{-1})
E_T	trap energy, erg (6.95×10^{-13} times energy in kcal-mole^{-1})
f	limiting conductance of valve insert, cm^3-s^{-1}
J	flux density, cm^{-2}-s^{-1}
K	permeability, cm^{-1}-s^{-1}
k	Boltzmann's constant, 1.38×10^{-16} erg-K^{-1}
$N(E)$	distribution of Auger electrons
P	pressure, dyne-cm^{-2} (1.33×10^3 times pressure in torr)
P_d	pressure at UHV interface, dyne-cm^{-2}(1.33×10^3 times pressure in torr)
P_0	high-side pressure, dyne-cm^{-2} (1.33×10^3 times pressure in torr)
P_p	pump pressure, dyne-cm^{-2} (1.33×10^3 times pressure in torr)
QMS	quadrupole mass spectrometer
R	universal gas constant, 8.314×10^7 erg-mol^{-1}-K^{-1}
S	solubility, cm^{-3}
T	temperature, K
t	time, s
UHV	ultrahigh vacuum
V	volume of measurement chamber, cm^3
x	variable distance through membrane, cm

Subscripts:

EM	Eichenauer and Mueller

eff effective

eq equilibrium

Analysis

The development of the equations (ref. 8) used for the determination of the permeability and the diffusivity is given in the appendix. The permeability K can be found from equation (A8)

$$J_{eq} = \frac{K P_0^{1/2}}{d}$$

Since the equilibrium flux J_{eq} through the membrane is related to the equilibrium pressure P_{eq} by

$$J_{eq} = \frac{P_{eq} f}{AkT} \tag{1}$$

where f is the limiting conductance of the valve insert, k is Boltzmann's constant, T is the gas temperature, and A is the membrane area, then

$$K = \frac{P_{eq} f d}{P_0^{1/2}} \tag{2}$$

The diffusivity data can be found in the following manner. The time varying total flux $AJ(t)$ and pressure $P(t)$ within the system are related by

$$V \frac{dP(t)}{dt} = AkT\, J(t) - f[P(t) - P_p(t)] \tag{3}$$

where V is the volume of the measurement chamber and $P_p(t)$ is the time-varying pressure within the pump.

Since $P(t) >> P_p(t)$, then

$$J(t) = \left(\frac{V}{AkT}\right) \frac{dP(t)}{dt} + \left(\frac{f}{AkT}\right) P(t) \tag{4}$$

A worst case condition occurs at high temperatures when $\frac{dP(t)}{dt}$ is greatest, but even at 800°C the ratio of the first term on the right-hand side to the second term is less than ~0.02, so the flux can be written as

$$J(t) \approx \left(\frac{f}{AkT}\right) P(t) \tag{5}$$

We can now say that

$$\frac{J(t)}{J_{eq}} \approx \frac{P(t)}{P_{eq}} \tag{6}$$

The ratio of (A11) to (A8) combined with equation (6) gives

$$\frac{P(t)}{P_{eq}} = -2 \sum_{1}^{\infty} (-1)^n \exp\left(-\frac{D n^2 \pi^2 t}{d^2}\right) \tag{7}$$

where D is the diffusivity. Experimentally, the time for $\frac{P(t)}{P_{eq}} = 0.1$ can be determined, and we can find D by numerical iteration of equation (7).

Experiment

Membrane Preparation

The permeation membranes (99.9999+ percent vacuum-melted Ag) were spark machined into the disk geometry shown in figure 1. The membrane surfaces were prepared as shown in the following table.

Step	Method
1. Polished	30-μm grit finish
2. Degreased	Laboratory detergent in ultrasonic cleaner
3. Rinsed	Deionized H_2O in ultrasonic cleaner
4. Chemically cleaned	4 parts HNO_3 to 1 part deionized H_2O
5. Rinsed	Deionized H_2O
6. Dried	Oil-free and filtered N_2

Attempts at electropolishing the Ag were only successful with about one out of five membranes and left as much or more surface contamination than the chemical cleaning with the HNO_3 solution. Auger electron spectroscopy (AES) analysis of the surface conducted after the cleaning procedure was completed is shown in figure 2(a) and closely resembles the spectrum of a sputter-cleaned Ag surface. Small contaminant levels of S, Cl, C, and O can be observed, but the S, Cl, and C peaks were easily removed during the first few permeation runs of oxygen through the membrane (ref. 9).

The grain structure of the membranes studied in this work is shown in figure 2(b). The grain growth of the Ag membranes was stabilized during the prerun vacuum degassing before oxygen was admitted, to insure maximum growth of the grains. The grain size distribution runs from approximate diameters of 1 mm to 5 mm with the mean diameter about 1.75 mm. Grain boundary densities determined by the linear intercept method were found to be 0.25 grains/mm^2. Figure 2(b) also shows that a substantial amount of twinning occurred from the long periods at elevated temperatures (400°–800°C). These defects, as well as the grain boundaries and dislocations, can also serve as transport paths.

Apparatus

Figure 3 is a schematic that represents the UHV permeation system. During bakeout, valve A was open (8 l/s) to facilitate maximum pumping speed to the main ion pump. After bakeout and during permeation runs, the valve was in the closed position, which provided a calibrated conductance of 0.7 l/s for oxygen flow through the valve (see detail of valve A in fig. 3) and thus permitted the establishment of an equilibrium pressure. Note also detail B which shows the Ag membrane heater assembly. The 304L stainless steel hardware that constituted the system envelope was previously vacuum fired at 600°C for 16 h to minimize the hydrogen outgassing rate. The gas pressure was monitored both by a quadrupole mass spectrometer (QMS) and by an ion gage and indicated that the ultimate pressure of the system was in the 10^{-11} torr range. Note also in figure 3 that the high-pressure side of the membrane was ion pumped to permit appropriate cleanup of the high-pressure side of the membrane surface and of the oxygen supply line.

The background gas spectra at room temperature, before and after introducing 10 torr oxygen into the high-pressure side of the system, appeared to be normal for stainless steel systems that have been vacuum fired and then baked out for several days. There was no significant O_2 signal and no change observed in the signal even when the high-side pressure was increased to 100 torr O_2. (See fig. 4(a).) However, as shown in figure 4(b), the O_2 peak substantially increased and became the dominant signal when the Ag membrane was heated. The data shown in figure 4(b) correspond to equilibrium conditions for a Ag temperature of 750°C.

Procedure

After vacuum degassing the membrane at 800°C, oxygen was admitted to the high-pressure side (~150 torr), equilibrium flow was established, and then the upstream pressure was removed to determine the pressure decay in the measurement chamber. After several cycles of this procedure to clean the membrane on both faces, data were taken at 25°C increments over the temperature range of 400°–800°C by monitoring the signals of both the ion gage and QMS through a logarithmic picoammeter and strip chart recorder. The emission current of each instrument was maintained much lower than normal at 0.4 mA and 0.5 mA, respectively, to minimize instrument pumping.

Figure 5 shows representative data for oxygen breakthrough to equilibrium (T_{Ag} = 600°C, P_0 = 150 torr O_2) and then pressure decay (T_{Ag} = 600°C, $P_0 \rightarrow 0$ torr O_2). The pressure decay method was used to calculate the diffusivities for O/Ag, since it was experimentally simpler to establish equilibrium for a given P_0 and then open a pump valve to reduce the pressure to $P_0 = 0$ than to "shock" a hot Ag membrane with a differential pressure of up to 150 torr. In this method it was observed that the diffusivity data were independent of pressure for all pressures above 50 torr, although the reason for the weak dependency below this value is not yet clear. The curvature that occurs after the linear decay in the signal is due to the incorporation of oxygen into the stainless steel walls of the vacuum system at equilibrium. When the upstream side is evacuated, a linear decay on a $\ln P(t)$ versus time plot is predicted by equation (7); but ultimately, the data begin to curve because the charged walls now see an opposite concentration gradient, which causes oxygen to desorb into the gas phase. This increase in oxygen gas flux results in an increased ultimate pressure.

At the higher temperatures studied, the vapor pressure of the Ag is sufficient to cause some material loss from the membrane. For example, at 800°C the vapor pressure is approximately 5×10^{-5} torr, which translates into a sublimation rate of 0.01 mm/h. This represents a significant mass loss and required corrections for each experimental run.

This procedure was used to study three different Ag membranes. The high-purity oxygen supply was also changed several times to insure repeatability.

Results and Discussion

Permeation coefficients were calculated from equation (2) and are presented in figure 6 in the form of an Arrhenius plot. The linearity of the data is quite good and was repeated over six separate runs. Several initial runs were required, however, before the data became repeatable, presumably because of contaminant removal by the oxygen. A comparison with the apparent permeability determined by Eichenauer and Mueller (ref. 2) shows that the data reported here are considerably lower in magnitude (by a factor of 3.2) but similar in slope. One possible explanation for the lower magnitude is that grain boundary diffusion is the primary mechanism of oxygen transport. Silver is well known to be very sensitive to impurities restricting grain growth, since the segregation of these impurities to the grain boundaries tends to slow down or stop intergranular transfer of Ag atoms from smaller to larger grains. This would indicate many more grain boundaries and therefore many more transport paths, which would mean a larger permeation rate. Although there is virtually no information on the microstructure of the Ag samples used by others, it is almost a certainty that

less pure Ag would result in substantially smaller grains. The highest purity Ag studied was reported by Eichenauer and Mueller (99.99 percent vacuum melted at an ultimate pressure of $\sim 10^{-3}$ torr) and was far more contaminated than the Ag used in this work (99.9999+ percent vacuum melted at an ultimate pressure of $\sim 10^{-8}$ torr).

The permeability equation determined from a least-squares fit of the data in figure 6 is

$$K = 1.01 \times 10^{18} \exp\left[\frac{-21\,870}{RT}\right] \text{cm}^{-1}\text{-s}^{-1} \qquad (8)$$

The activation energy (E_a = 21 870 cal/mole) associated with these data compares well with that of Eichenauer and Mueller. It is important to note that for all permeation data with high-side pressures of P_0 = 5, 10, 100, 150, 200, and 250 torr, the data fell on the same straight line, which agrees with Sievert's Law and the assumption that the O atoms move through the Ag in the atomic state.

As observed in the permeation data, changes in the diffusivity were observed as the membrane became more and more contaminant free, but after several runs the data became very repeatable. As shown in figure 7, a break in linearity occurs at ~630°C. The first few runs over the temperature range produced somewhat linear diffusivity plots, but subsequent data began to reveal the aforementioned break. Associated with this break was a very dramatic change in the QMS spectra. The first few runs showed significant CO and CO_2 peaks, but as shown in figure 4(b), these signals substantially declined in later runs. Unfortunately, the change in QMS spectra due to Ag cleanup was probably masked by the vacuum chamber wall cleanup, but the resulting spectra appear to be similar to that observed by Beavis (ref. 10). The equations determined from these plots are

$$D = 2.96 \times 10^{-3} \exp\left[\frac{-11\,050}{RT}\right] \text{cm}^2\text{-s}^{-1} \quad 630 \le T \le 800°C \qquad (9a)$$

$$D = 3.2 \times 10^{-2} \exp\left[\frac{-15\,330}{RT}\right] \text{cm}^2\text{-s}^{-1} \quad 400 \le T \le 630°C \qquad (9b)$$

In the higher temperature case, the value of the activation energy (E_a = 11 050 cal/mole) is almost exactly that obtained by Eichenauer and Mueller (E_a = 11 000 cal/mole). At temperatures below 630°C, however, the value of the activation energy (E_a = 15 330 cal/mole) is considerably higher.

Figure 8 shows the desorption of oxygen from the membrane (vacuum on both sides) observed during the increase in membrane temperature to 800°C. Note that at 630°C sufficient thermal energy exists so that the onset of vacuum desorption of oxygen from the membrane occurs and indicates that the oxygen atoms are probably migrating with an increased mobility within the grain boundaries. In the work of Eichenauer and Mueller, one can question what actually occurs below 600°C because of less pure conditions, lack of oxygen purging, and much larger sample dimensions (impurities in the grain boundaries would require a much longer time to migrate to the surface because of much larger dimensions). For example, sulfur segregation to the grain boundaries could substantially decrease the chemical affinity of the oxygen to the Ag, since it would interact with a more passive surface of chemisorbed S on Ag. In higher purity materials, the S content in the grain boundaries is less, which increases the oxygen interaction with more available Ag bonds. Mitchell et al. (ref. 11) have shown the effects of hydrogen trapping in copper due to the addition of substitutional impurities Er, Zr, and Ti. They noted no change in the permeability, even up to 4 atomic percent of Zr, but they did observe a significant decrease in the magnitude of the effective diffusivity (D_{eff} represents the effect of the trap in contrast to the D in pure Cu). Further, the slope of the D_{eff} (for all impurities) in an Arrhenius plot was also greater than for the D in the pure Cu and represents an increased activation energy because of the trap. Although we are concerned with interstitials and with far less impurity concentration, it is quite likely that a similar effect could be active in this work, especially since both substitutionals and interstitials often segregate to grain boundaries and behave in a similar manner. According to their analysis, the observed energy E is just the sum of the trap energy E_T and the activation energy E_A. One then obtains E_T = 4.28 kcal-mole^{-1} for the oxygen in the grain boundaries.

Grain boundary self-diffusion is well known in Ag and predominates lattice diffusion below 750°C for small grain material (ref. 12). The diffusion of oxygen in grain boundaries, therefore, might be prevalent as well, since it is a smaller atom and has less chemical affinity for Ag than Ag for itself. This behavior also suggests that lattice diffusion of oxygen probably does not predominate grain boundary diffusion until a temperature substantially in excess of 750°C is achieved and therefore might not be observed in this work.

If we now assume that grain boundary diffusion is the dominant mechanism for O transport in Ag, then we can further compare our work with that of Eichenauer and Mueller in the region above 630°C. Since our diffusivity values are approximately the

same, we can write the ratio of the permeabilities to be

$$\frac{K}{K_{EM}} = \frac{S}{S_{EM}} \tag{10}$$

where EM represents the values calculated by Eichenauer and Mueller. Now if the solubility S is defined as being directly proportional to the volume fraction f of grain boundaries in the solid, and the effects of traps are ignored, then

$$S = \alpha f \tag{11}$$

where α is the same constant for both cases. Equation (10) becomes

$$\frac{K}{K_{EM}} = \frac{f}{f_{EM}} \tag{12}$$

The ratio of permeabilities then requires that

$$\frac{f}{f_{EM}} \approx 3.2$$

This is consistent with the lower grain boundary densities in this work, which provide less grain boundary reservoirs for oxygen atoms for any given temperature.

The solubility of oxygen in Ag inferred from the DS product is

$$S = 3.41 \times 10^{19} P_0^{1/2} \exp\left[\frac{-10\,820}{RT}\right] \text{cm}^{-3} \quad 630° \le T \le 800°C \quad (P_0 \text{ in torr}) \tag{13a}$$

$$S = 3.16 \times 10^{18} P_0^{1/2} \exp\left[\frac{-6540}{RT}\right] \text{cm}^{-3} \quad 400° \le T \le 630°C \quad (P_0 \text{ in torr}) \tag{13b}$$

Equation (13a) can be compared with that of Eichenauer and Mueller, which is

$$S_{EM} = 1.42 \times 10^{20} P_0^{1/2} \exp\left[\frac{-11\,860}{RT}\right] \text{cm}^{-3} \quad (P_0 \text{ in torr})$$

which, as already indicated, represents a higher solubility than observed in this work.

The mechanism by which the oxygen moves through the grain boundaries at any temperature is quite complex and is not clearly understood. It is quite clear, however, that the vacuum desorption of oxygen shown in figure 8 represents some thermally activated change that occurs in the polycrystalline structure above 630°C. Surface studies have shown that the sticking coefficient of molecular oxygen on Ag is very low ($\sim 10^{-3}$ on the (110) face and $\sim 10^{-6}$ on the (111) face). It is also known that oxygen adsorbed on the (110) face is in the atomic state and quite stable below 310°C, but completely desorbs at temperatures greater than 450°C, which indicates a much stronger interaction than for molecules (refs. 13 and 14). Because the grain boundary is a much more disordered region, perhaps the oxygen atoms are even more strongly bound and require a higher temperature (630°C) before desorption can occur.

Concluding Remarks

The permeation of oxygen through large grain, high purity Ag is quite repeatable and quite linear over the temperature range 400°–800°C. The fact that the magnitude of K over this range is a factor of 3.2 less than that found by others studying substantially less pure material indicates strongly, although not conclusively, that oxygen permeates the membranes by grain boundary diffusion. The diffusivity data also are quite repeatable but exhibit two linear regions, one above and another below a critical temperature of 630°C. The high-temperature data (630°–800°C) have a similar activation energy to that reported by others but the low-temperature data (400°–630°C) have a higher activation energy. This is consistent with impurity trapping, most likely at the grain boundaries. Vacuum desorption of the oxygen was found to occur at a threshold of 630°C, which suggests the onset of desorption from the Ag and an increased mobility in the grain boundaries.

NASA Langley Research Center
Hampton, VA 23665-5225
July 20, 1987

Appendix

Permeation Analysis

The permeation of planar membranes is generally described by reference 8. If a diffusion coefficient independent of concentration C is assumed, then

$$\frac{\partial C}{\partial t}(x,t) = D\left[\frac{\partial^2 C(x,t)}{\partial x^2}\right] \tag{A1}$$

where x is the variable distance through the membrane.

The boundary conditions applied to this equation can be determined from the permeation process, which include (1) adsorption of the oxygen molecules on the high-pressure side; (2) dissociation of the molecules to atoms; (3) incorporation of the atoms into the interstices of the lattice, grain boundaries, or defects; (4) random walk migration through the membrane by means of (3); (5) emergence from solid solution at the vacuum interface and entry into an adsorbed state; (6) reassociation to molecules; and (7) desorption.

Normally the rate controlling step is that of (4), and equation (1) may be solved for the following boundary conditions:

$$C(x, t = 0) = g(x) \tag{A2}$$

$$C(x = 0, t) = SP_0^{1/2} = C_1 \text{ (Sievert's Law)} \tag{A3}$$

$$C(x = d, t) = SP_d^{1/2} = C_2 \text{ (Sievert's Law)} \tag{A4}$$

where $g(x)$ is an arbitrary function, d is the membrane thickness, S is the solubility, P_0 is the high-side pressure, and P_d is the pressure at the UHV interface, which is usually taken to be zero at the begining of the experiment. In equations (A3) and (A4) the 1/2 power was assumed, which indicates that the oxygen migrates through the solid as atoms. Considering the above conditions, the solution to equation (A1) is

$$C(x,t) = C_1 + (C_2 - C_1)\frac{x}{d} + \frac{2}{\pi}\sum_1^\infty \left[\frac{C_2 \cos n\pi - C_1}{n}\right] \sin\frac{n\pi x}{d} \exp\left(-\frac{Dn^2\pi^2 t}{d^2}\right)$$

$$+ \frac{2}{d}\sum_1^\infty \sin\frac{n\pi x}{d} \exp\left(-\frac{Dn^2\pi^2 t}{d^2}\right)\int_0^d g(x) \sin\frac{n\pi x}{d}\, dx \tag{A5}$$

Now, if at $t = 0$ vacuum is on both sides of the membrane, then $g(x) = 0$. If the upstream side of the membrane is pressurized, $C_1 = SP_0^{1/2}$, $C_2 = 0$, and equation (5) becomes

$$C(x,t) = C_1\left[1 - \frac{x}{d} - \frac{2}{\pi}\sum_{n=1}^\infty \frac{1}{n}\sin\frac{n\pi x}{d} \exp\left(-\frac{Dn^2\pi^2 t}{d^2}\right)\right] \tag{A6}$$

The gas flux J then is

$$J(x = d, t) = -D\left(\frac{\partial C}{\partial x}\right)_{x=d}$$

$$= \frac{DSP_0^{1/2}}{d}\left[1 + 2\sum_1^\infty (-1)^n \exp\left(-\frac{Dn^2\pi^2 t}{d^2}\right)\right] \tag{A7}$$

which for large time is

$$J(x = d,\ t \to \infty) = \frac{DSP_0^{1/2}}{d} = \frac{KP_0^{1/2}}{d} = J_{eq} \tag{A8}$$

where the permeability $K = DS$.

In order to determine the diffusivity following the establishment of a steady-state permeation rate, the upstream or high-pressure side can be reduced to zero such that $C_1 = C_2 = 0$ and the concentration through the membrane with reset time $t = 0$ is

$$C(x, t = 0) = g(x) = SP_0^{1/2}\left(1 - \frac{x}{d}\right) \tag{A9}$$

thus equation (A5) becomes

$$C(x,t) = \frac{2}{d}\sum_1^\infty \frac{\sin n\pi x}{d}\ \exp\left(-\frac{Dn^2\pi^2 t}{d^2}\right)\int_0^d SP_0^{1/2}\left(1 - \frac{x}{d}\ \sin\frac{n\pi x}{d}\right)\ dx$$

which yields

$$C(x,t) = \frac{2SP_0^{1/2}}{\pi}\sum_{n=1}^\infty \frac{1}{n}\ \sin\frac{n\pi x}{d}\ \exp\left(-\frac{Dn^2\pi^2 t}{d^2}\right) \tag{A10}$$

and the flux is

$$J(x = d, t) = \frac{KP_0^{1/2}}{d}\left[-2\sum_1^\infty (-1)^n\ \exp\left(-\frac{Dn^2\pi^2 t}{d^2}\right)\right] \tag{A11}$$

Now if $Dt \geq 1 \times 10^{-4}$, then the ratio of the first and second terms is $J_{n=2}/J_{n=1} \approx 0.01$ and $J(x = d, t)$ can then be written as

$$J(x = d, t) = \frac{2KP_0^{1/2}}{d}\ \exp\left(-\frac{D\pi^2 t}{d^2}\right) \tag{A12}$$

Dividing equation (A12) by (A8) gives the normalized flux

$$\frac{J}{J_{eq}} = 2\ \exp\left(-\frac{D\pi^2 t}{d^2}\right) \tag{A13}$$

References

1. Outlaw, R. A.; Peregoy, W. K.; Hoflund, Gar B.; and Corallo, Gregory R.: *Electron Stimulated Desorption of Atomic Oxygen From Silver*. NASA TP-2668, 1987.
2. Eichenauer, Walter; and Mueller, Gudrun: Diffusion and Solubility of Oxygen in Silver. *Zeitschrift fuer Metallkunde*, Bd. 53, 1962, pp. 321–324.
3. Ramanarayanan, T. A.; and Rapp, R. A.: The Diffusivity and Solubility of Oxygen in Liquid Tin and Solid Silver and the Diffusivity of Oxygen in Solid Nickel. *Metall. Trans.*, vol. 3, no. 12, Dec. 1972, pp. 3239–3246.
4. Rickert, Hans; and Steiner, Rolf: Elektrochemische Messung der Sauerstoffdiffusion in Metallen bei Höheren Temperaturen. *Zeitschrift für Physikalische Chemie,* Bd. 49, Heft 3/5, May 1966, pp. 127–137.
5. Kolosov, E. N.; Starkovskii, N. I.; and Gryaznov, V. M.: Mass-Spectrometric Study of the Isotopic Composition of Oxygen Diffused Through a Silver Membrane. *Zhurnal Fizicheskoi Khimii,* vol. 48, no. 7, 1974, pp. 1861–1862.
6. Gryaznov, V. M.; Gul'yanova, S. G.; and Kanizius, S.: Diffusion of Oxygen Through a Silver Membrane, *Russian J. Phys. Chem.*, vol. 47, no. 10, 1973, pp. 1517–1518.
7. Coles, R. E.: The Permeability of Silver to Oxygen. *British J. Appl. Phys.*, vol. 14, 1963, pp. 342–344.
8. Perkins, W. G.: Permeation and Outgassing of Vacuum Materials. *J. Vac. Sci. & Technol.*, vol. 10, no. 4, July/Aug. 1973, pp. 543–556.
9. Rovida, G.; Pratesi, F.; Maglietta, M.; and Ferroni, E.: Chemisorption of Oxygen on the Ag(111) Surface. *Surf. Sci.*, vol. 43, no. 1, May 1974, pp. 230–256.
10. Beavis, L. C.: Oxygen Permeation Through Silver. *Rev. Sci. Instrum.*, vol. 43, no. 1, Jan. 1972, pp. 122–127.
11. Mitchell, D. J.; Harris, J. M.; Patrick, R. C.; Boespflug, E. P.; and Beavis, L. C.: Deuterium Permeation Through Copper With Trapping Impurities. *J. Appl. Phys.*, vol. 53, no. 2, Feb. 1982, pp. 970–978.
12. Hoffman, R. E.; and Turnbull, D.: Lattice and Grain Boundary Self-Diffusion in Silver. *J. Appl. Phys.*, vol. 22, no. 5, May 1951, pp. 634–639.
13. Engelhardt, H. A.; and Menzel, D.: Adsorption of Oxygen on Silver Single Crystal Surfaces. *Surf. Sci.*, vol. 57, no. 2, July 1976, pp. 591–618.
14. Campbell, Charles T.: Atomic and Molecular Oxygen Adsorption on Ag(111). *Surf. Sci.*, vol. 157, no. 1, July 1985, pp. 43–60.

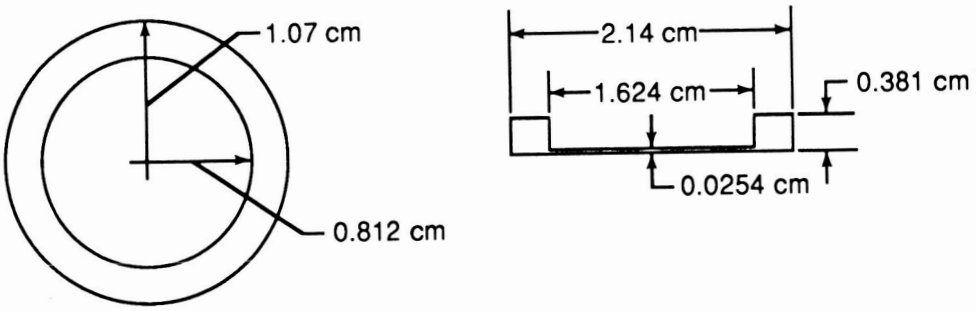

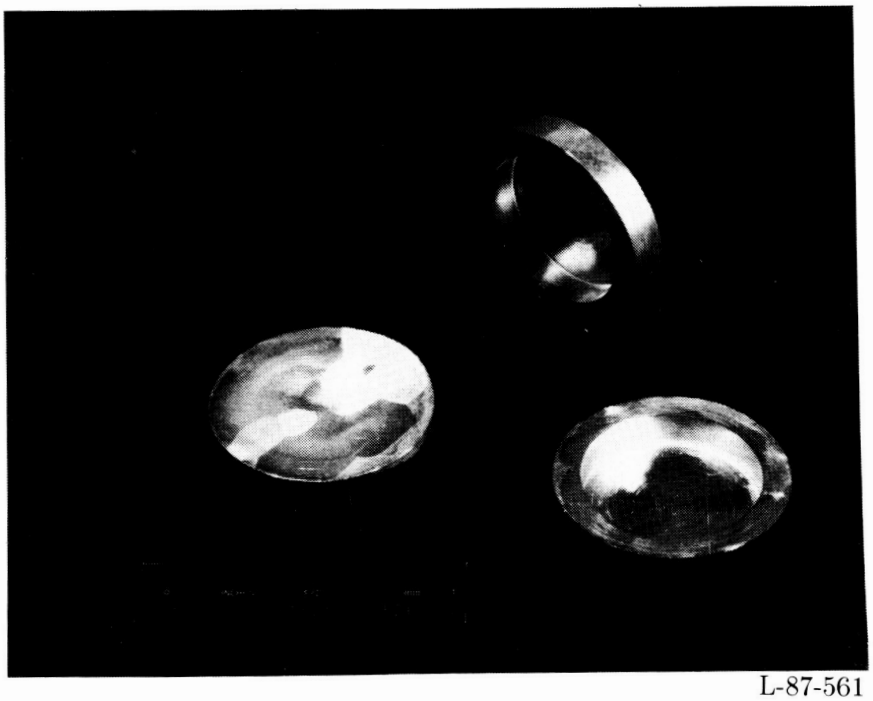

L-87-561

Figure 1. Geometry of 99.9999+ percent Ag permeation membranes.

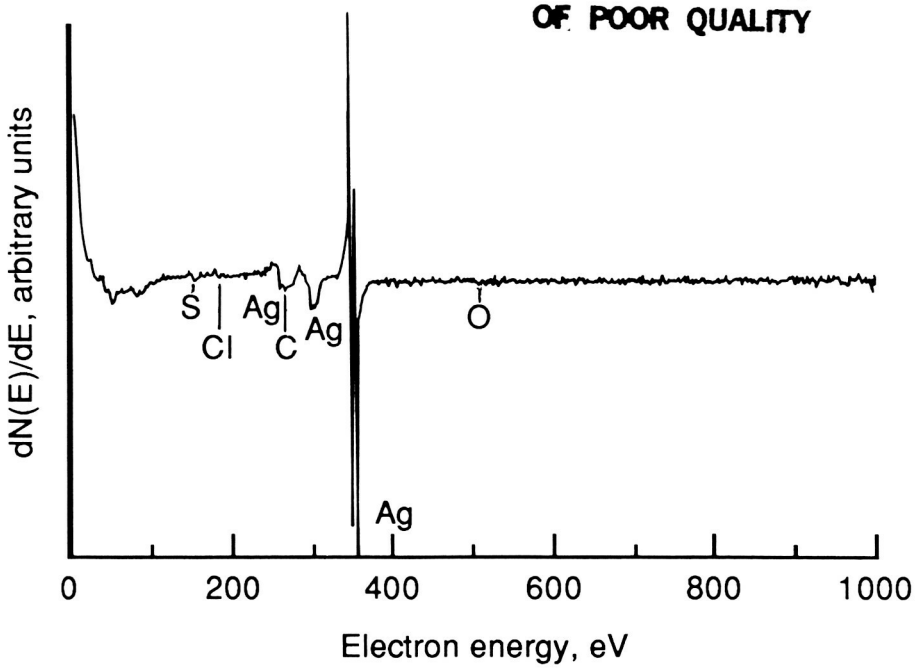

(a) AES survey of Ag membranes after polishing and chemical cleaning.

L-87-562

(b) Micrograph of Ag membrane (×15.2).

Figure 2. Ag membranes used in experiment.

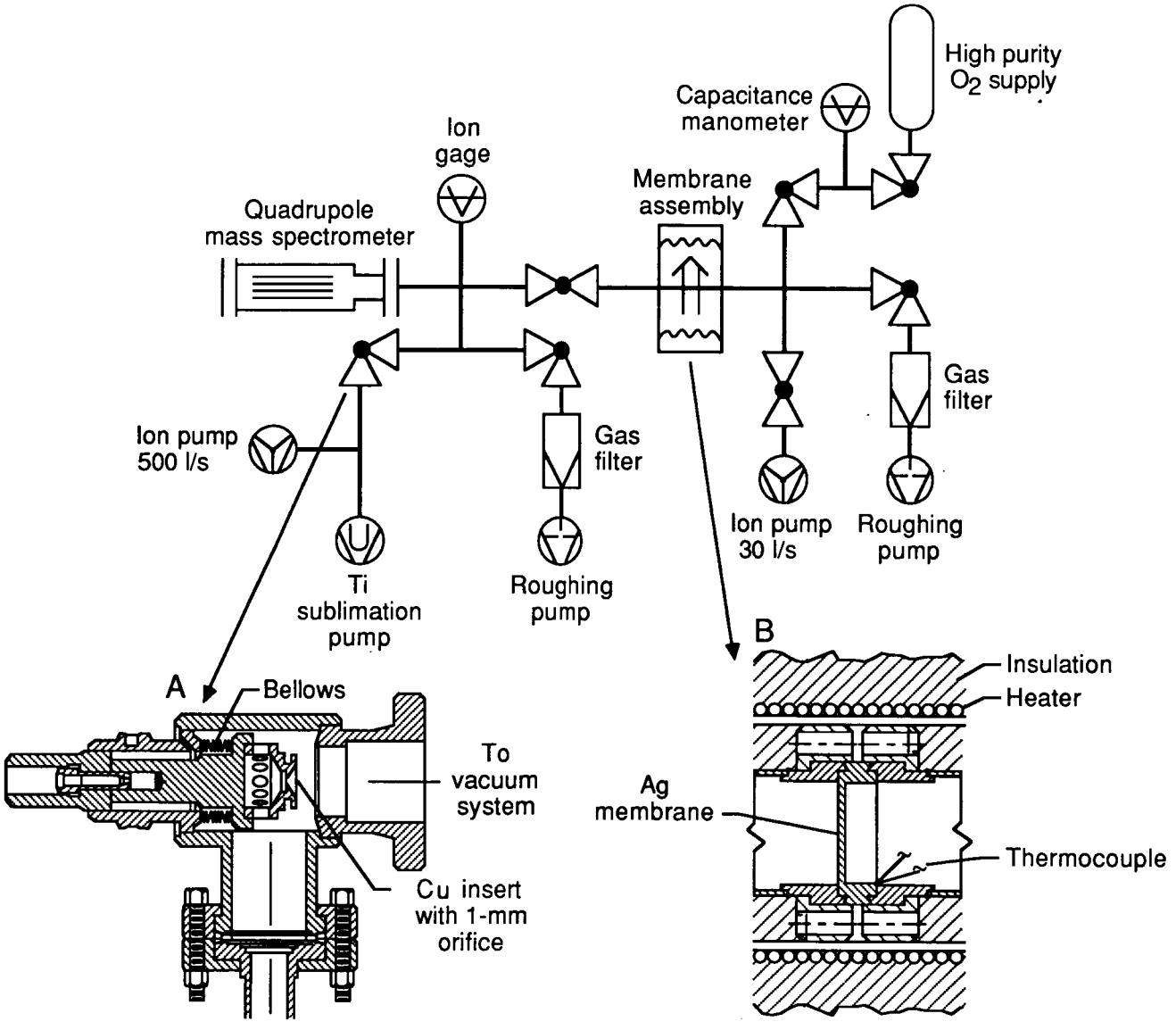

Figure 3. Schematic of UHV permeation system showing details (A), conductance limiting valve, and (B), miniflange geometry with permeation membrane.

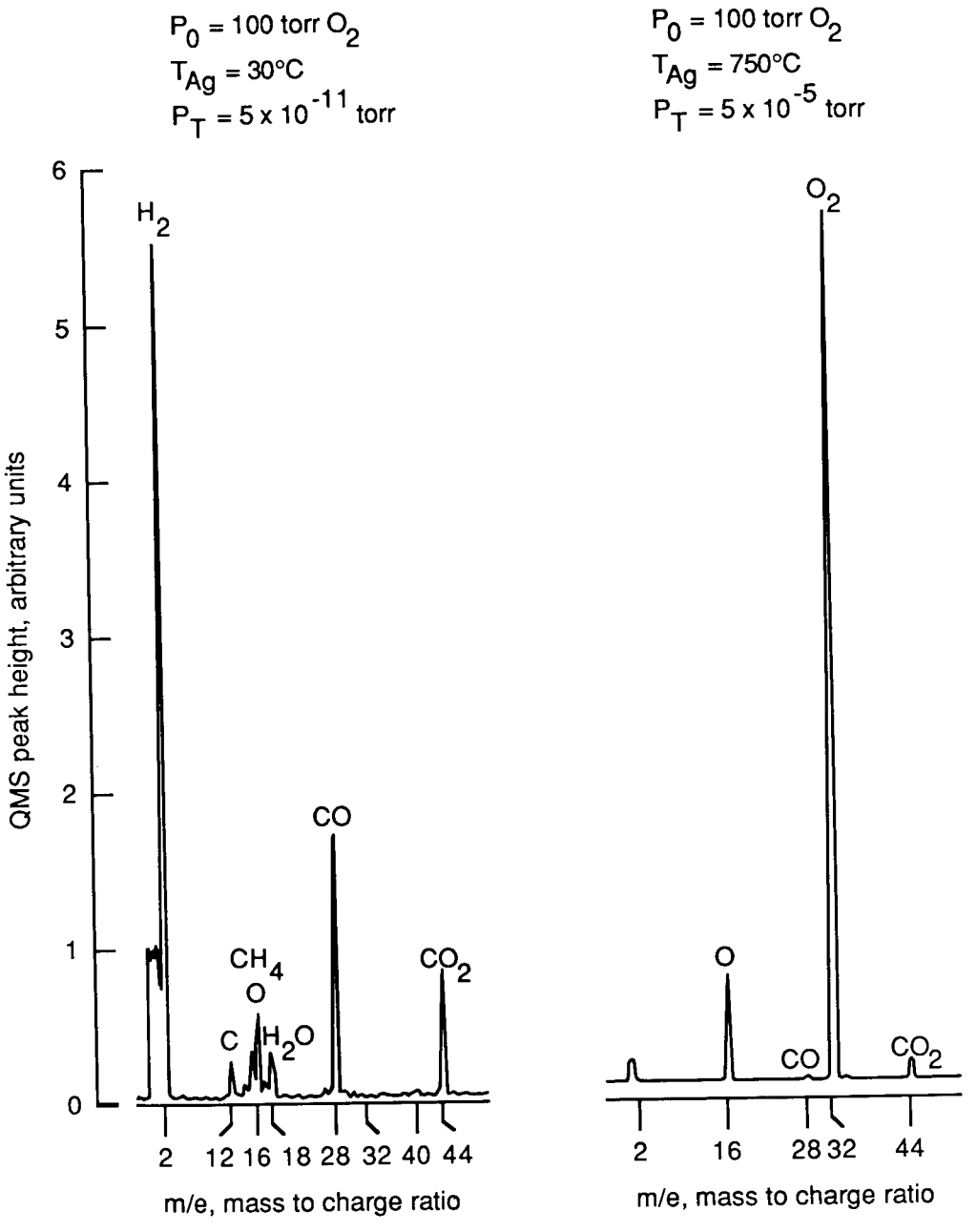

(a) Ag membrane at room temperature; P_0 = 100 torr O_2 (upstream pressure).

(b) Ag membrane at 750°C; P_0 = 100 torr O_2 (upstream pressure).

Figure 4. QMS spectra of system.

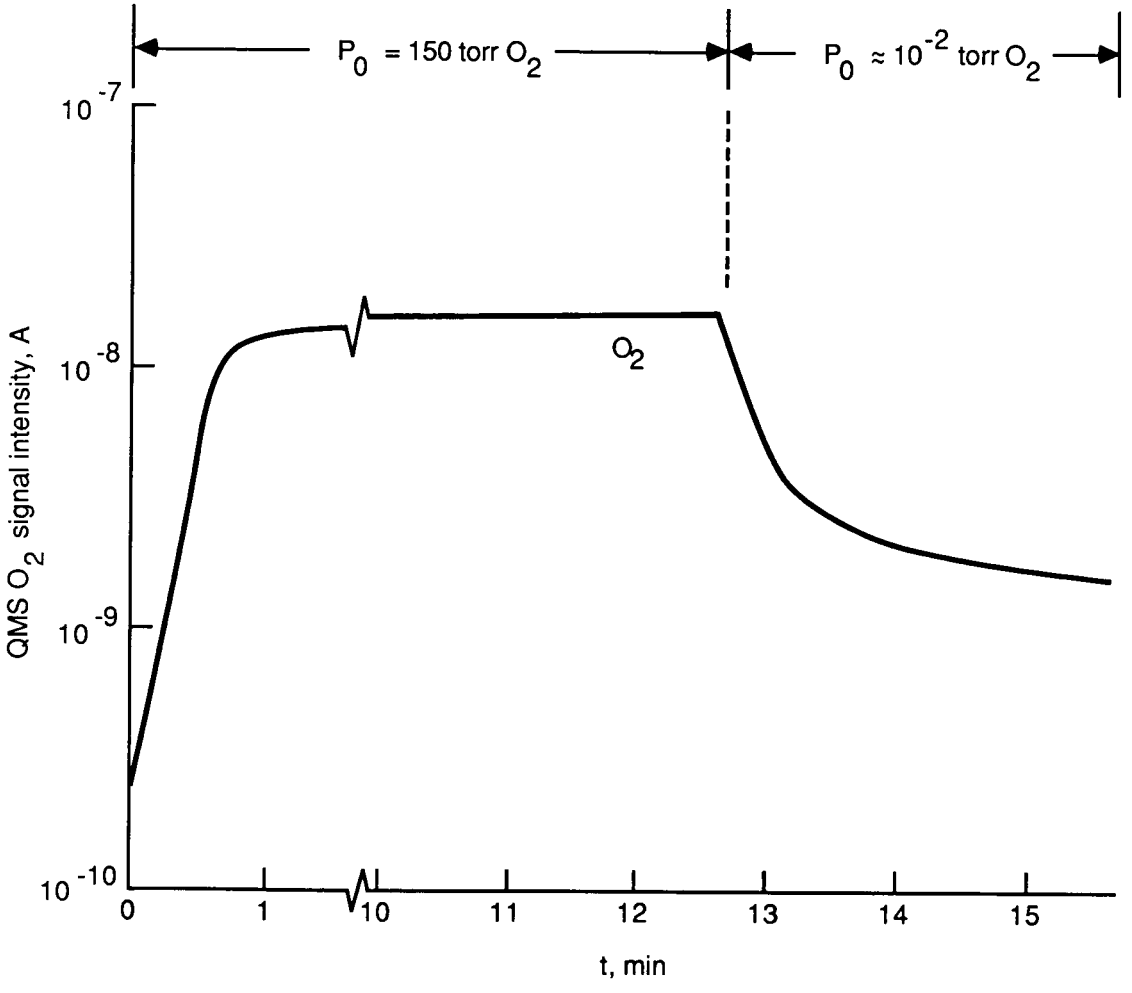

Figure 5. Breakthrough and decay of oxygen through Ag membrane ($T = 600°C$).

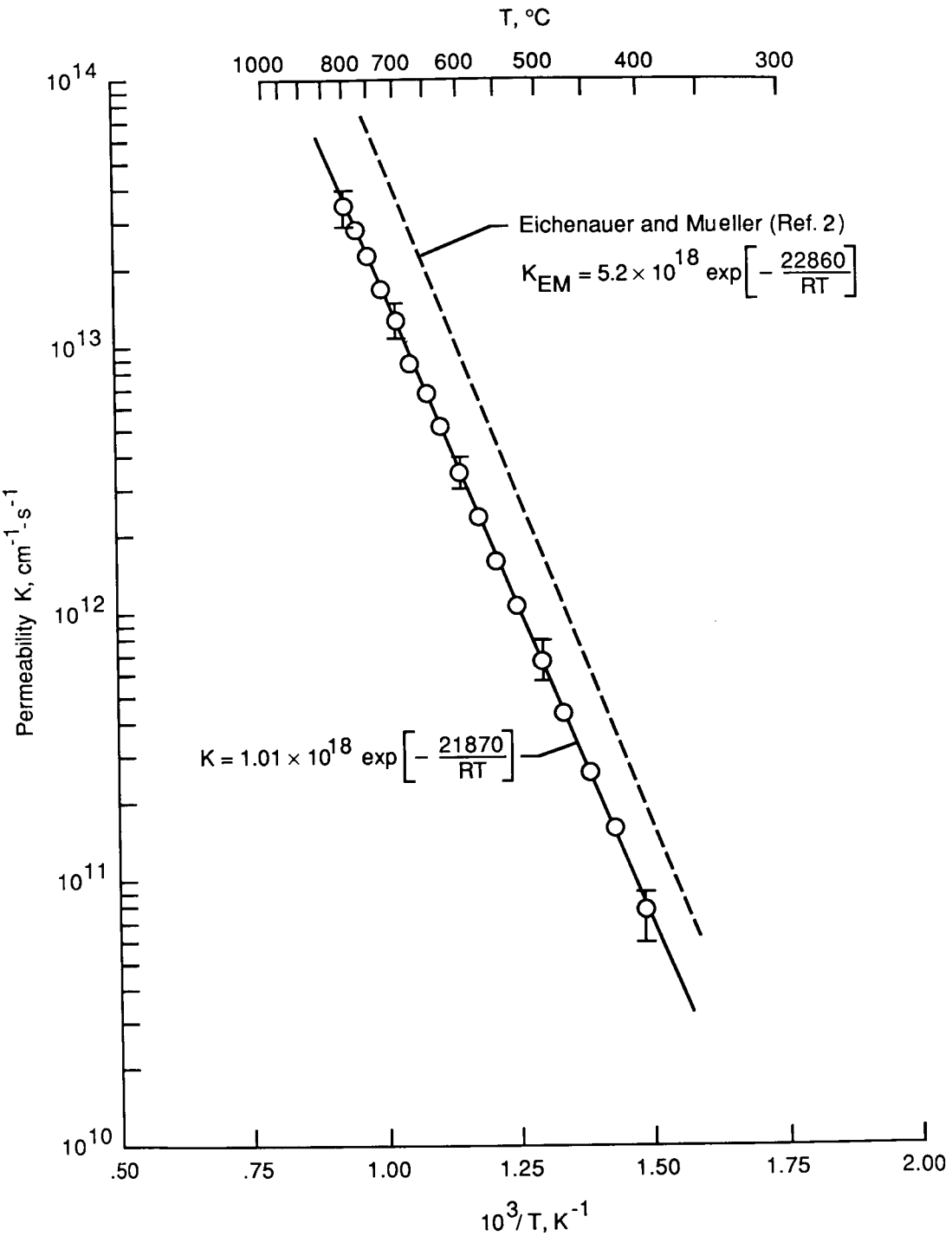

Figure 6. Arrhenius plot of permeation data compared with that of reference 2.

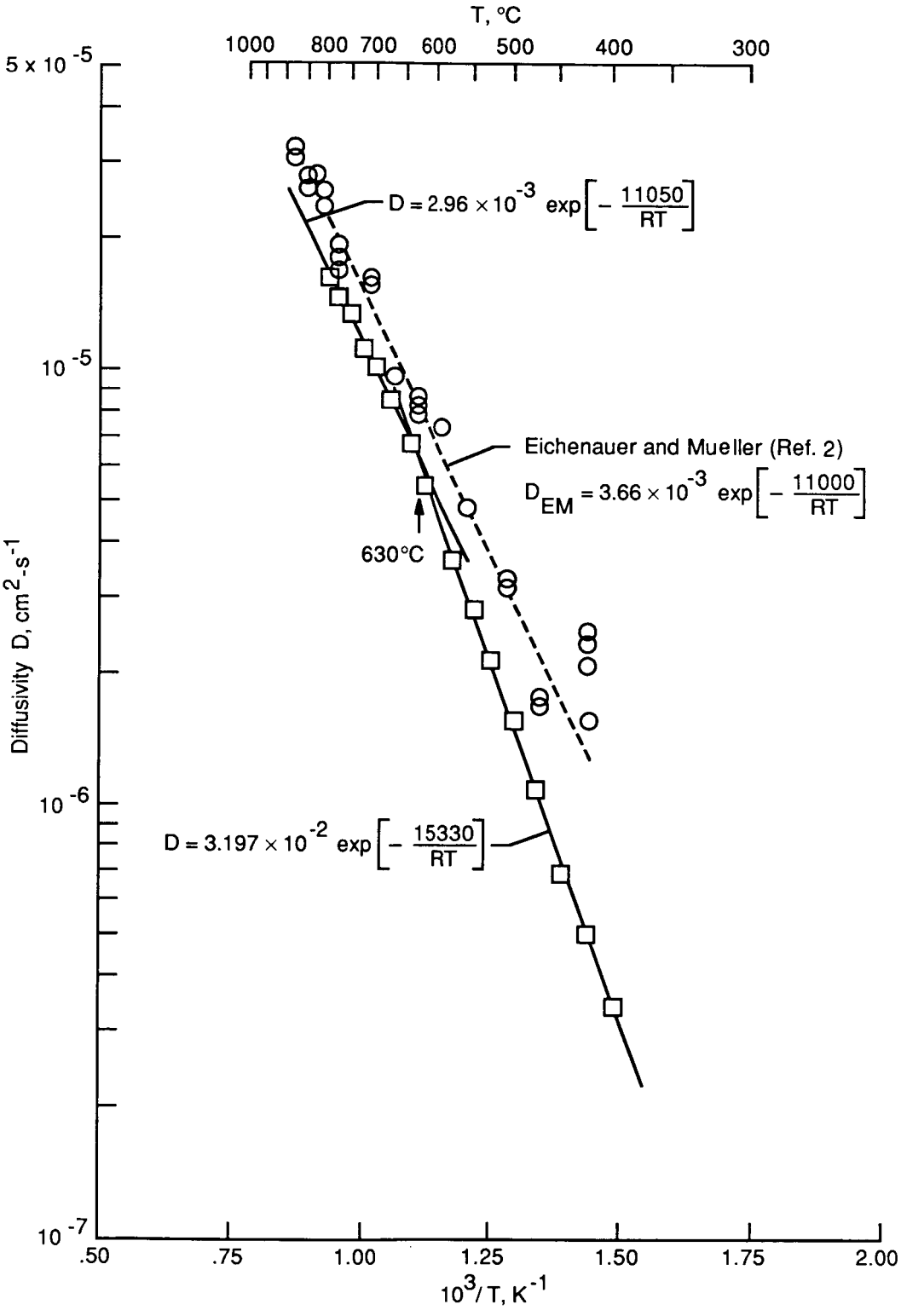

Figure 7. Arrhenius plot of diffusivity data compared with that of reference 2.

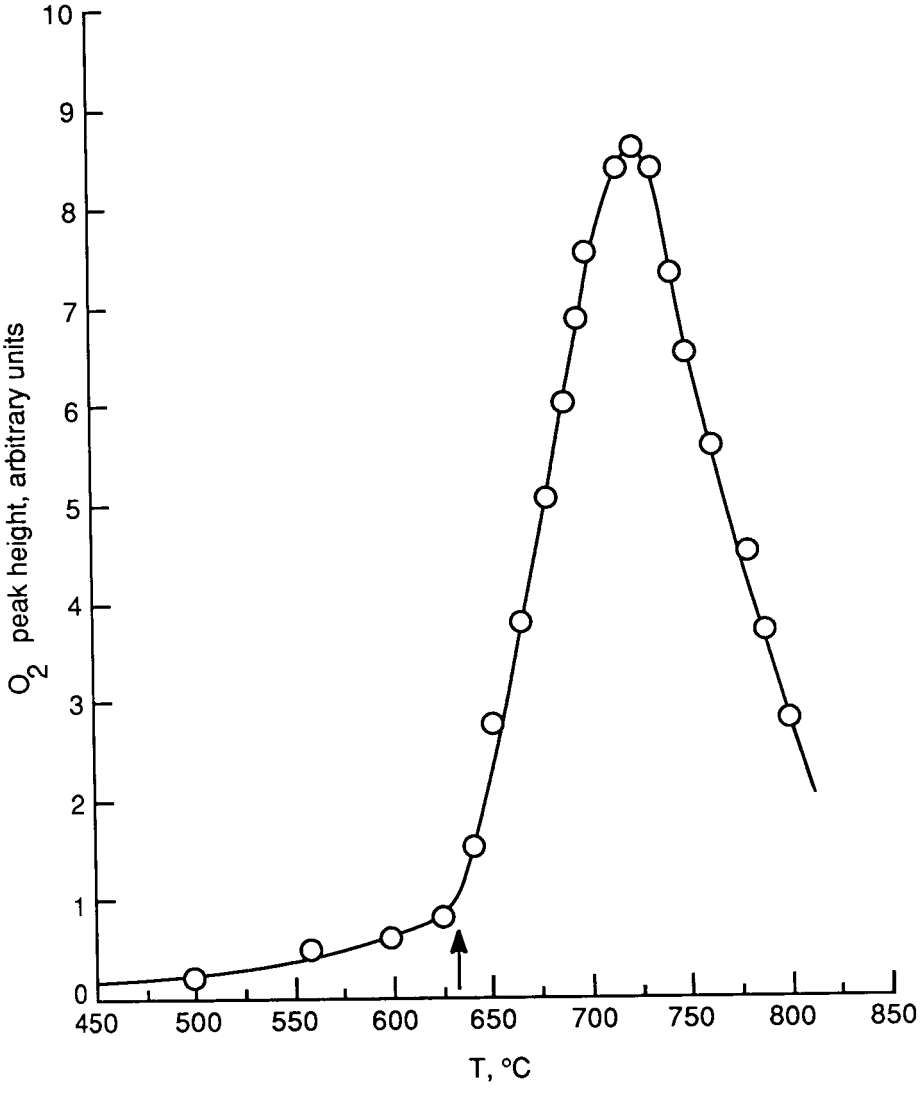

Figure 8. Vacuum desorption of oxygen from Ag membrane for $dT/dt = 4\text{K/min}$. Arrow indicates onset of vacuum desorption.

NASA
National Aeronautics and Space Administration

Report Documentation Page

1. Report No.	2. Government Accession No.	3. Recipient's Catalog No.
NASA TP-2755		

4. Title and Subtitle	5. Report Date
Permeation of Oxygen Through High Purity, Large Grain Silver	September 1987
	6. Performing Organization Code
7. Author(s)	8. Performing Organization Report No.
R. A. Outlaw, W. K. Peregoy, and Gar B. Hoflund	L-16305
9. Performing Organization Name and Address	10. Work Unit No.
NASA Langley Research Center Hampton, VA 23665-5225	307-51-07-01
	11. Contract or Grant No.
12. Sponsoring Agency Name and Address	13. Type of Report and Period Covered
National Aeronautics and Space Administration Washington, DC 20546-0001	Technical Paper
	14. Sponsoring Agency Code

15. Supplementary Notes

R. A. Outlaw and W. K. Peregoy: Langley Research Center, Hampton, Virginia.
Gar B. Hoflund: University of Florida, Gainesville, Florida.

16. Abstract

The permeation of high purity, large grain Ag membranes by oxygen has been studied over the temperature range 400°–800°C. The permeability was found to be quite linear and repeatable, but the magnitude was 3.2 times smaller than that determined by past research. Since previous investigators studied substantially less pure Ag and conducted experiments within much poorer vacuum environments (which indicates that their grain boundary density was much greater), the data presented here suggest oxygen transport through the membrane is primarily by grain boundary diffusion. The diffusivity measurements were found to exhibit two distinct linear regions, one above and one below a critical temperature of 630°C. The high-temperature data have an activation energy (11.1 kcal-mole^{-1}) similar to that reported by others, but the low-temperature data have a higher activation energy (15.3 kcal-mole^{-1}), which can be explained by impurity trapping in the grain boundaries. Vacuum desorption of the oxygen-saturated Ag was found to occur at a threshold of 630°C, which is consistent with the onset of increased mobility within the grain boundaries.

17. Key Words (Suggested by Authors(s))	18. Distribution Statement
Permeation Oxygen Silver Grain boundaries	Unclassified—Unlimited Subject Category 26

19. Security Classif.(of this report)	20. Security Classif.(of this page)	21. No. of Pages	22. Price
Unclassified	Unclassified	17	A02

NASA FORM 1626 OCT 86 NASA-Langley, 1987
For sale by the National Technical Information Service, Springfield, Virginia 22161-2171